

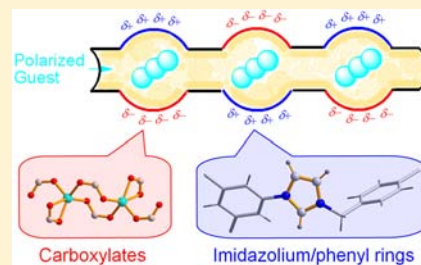
Two-Dimensional Charge-Separated Metal–Organic Framework for Hysteretic and Modulated Sorption

Sujuan Wang, Qiuli Yang, Jianyong Zhang,* Xuepeng Zhang, Cunyuan Zhao, Long Jiang, and Cheng-Yong Su*

MOE Laboratory of Bioinorganic and Synthetic Chemistry/KLGHEI of Environment and Energy Chemistry, Lehn Institute of Functional Materials, School of Chemistry and Chemical Engineering, Sun Yat-Sen University, Guangzhou 510275, China

Supporting Information

ABSTRACT: A charge-separated metal–organic framework (MOF) has been successfully synthesized from an imidazolium tricarboxylate ligand, *N*-(3,5-dicarboxylphenyl)-*N'*-(4-carboxylbenzyl)imidazolium chloride (DCPCBImH₃Cl), and a zinc(II) dimeric secondary building unit, namely, DCPCBim-MOF-Zn, which shows an unprecedented 3,6-connected two-dimensional net topology with the point (Schläfli) symbol (4².6)₂(4⁴.6⁹.8²). The framework contains one-dimensional highly polar channels, and density functional theory calculations show that positive charges are located on the imidazolium/phenyl rings and negative charges on the carboxylate moieties. The charge-separated nature of the pore surface has a profound effect in their adsorption behavior, resulting in remarkable hysteretic sorption of various gases and vapors. For CO₂, the hysteretic sorption was observed to occur even up to 298 K. Additionally, trace chloride anions present in the pore channels are able to modulate the gas-sorption behavior.



INTRODUCTION

The rational design and synthesis of metal–organic frameworks (MOFs) are attracting considerable attention because of their potential application in storage, separation, and heterogeneous catalysis.¹ The ability to rationally select the components is expected to control the function, e.g., pore surface functions. The introduction of electrostatic force sites into the MOF pore surface is an effective technique for enhancing the adsorption of guest molecules compared with dispersion interactions. Nevertheless, the fabrication of polar microporous MOFs remains a significant challenge even though several strategies have been reported for electrostatic force involvement.² So far, the electrostatic interactions are known to be able to be introduced into MOF structures through various methods like metal-ion doping,³ polar species modification,⁴ and charge separation.⁵

As a group of ligands potentially suitable for creating charge-separated MOFs, cationic azolium compounds (N-heterocyclic carbene precatalysts), which bear carboxylate donors, are of interest. In addition, when azolium salts are incorporated into MOFs, these organic groups may generate pockets that are suitable for binding anionic guests or enhancing the physisorption of small molecules and may be available for tethering catalytically active metal complexes by unmasking the azolium moiety.⁶ For example, two-dimensional (2D) or three-dimensional frameworks containing azolium sites can anchor Pd^{II} or Cu^I cations for potential catalytic application.⁷ These MOFs have rigid and porous structures to overcome the standing problem of low porosity.⁸ However, all of the resulting MOFs have overall charged frameworks and contain counterions in the pore channels for charge compensation, so that guest-molecule inclusion may be blocked, the porosity is

reduced, and the framework is not easily evacuated. Herein we report a 2D MOF based on an imidazolium tricarboxylate ligand. The overall charge of the framework is in balance, and the framework has one-dimensional (1D) pore channels with charge-separated nature that have a profound effect on their hysteretic sorption behavior.

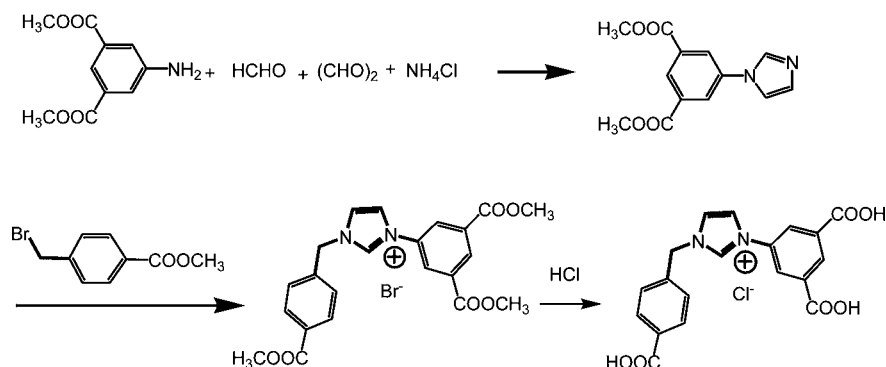
RESULTS AND DISCUSSION

Synthesis and Crystal Structure. A new ligand, *N*-(3,5-dicarboxylphenyl)-*N'*-(4-carboxylbenzyl)imidazolium chloride (DCPCBImH₃Cl), was synthesized as depicted in Scheme 1. The imidazole ring was formed via the synthesis of a diazabutadiene intermediate from dimethyl 5-aminoisophthalate, ammonium chloride, and glyoxal in equivalent molar, before cyclization with formaldehyde. Subsequently, the reaction of methyl 4-(bromomethyl)benzoate with dimethyl 5-(1*H*-imidazol-1-yl)isophthalate proceeded smoothly in MeCN to give the trimethyl ester of imidazolium bromide in good yield (66%). The compound was isolated as its bromide salt. Acid-catalyzed hydrolysis of the trimethyl ester gave the target imidazolium tricarboxylic acid as a chloride salt, DCPCBImH₃Cl. The mild solvothermal reaction of DCPCBImH₃Cl and Zn(NO₃)₂·6H₂O with a metal/ligand ratio of 2:1 in *N,N*-dimethylformamide (DMF)/H₂O (3:1, v/v) at 80 °C afforded colorless crystalline products of {Zn₂(DCPCBIm)₂·DMF}_n (DCPCBim-MOF-Zn).

Single-crystal X-ray diffraction reveals that DCPCBim-MOF-Zn crystallizes in the monoclinic space group *C2/c*. The

Received: August 14, 2012

Published: March 26, 2013

Scheme 1. Synthesis of DCPCBimH₃Cl

asymmetric unit consists of one Zn ion and one DCPCBim ligand. The central Zn^{II} ion is five-coordinated by five O atoms (Zn–O 1.92–2.44 Å) from four different ligands. Two carboxylates bridge two Zn atoms to form a Zn₂ dimeric secondary building unit (SBU). Each Zn₂ SBU binds with six different DCPCBim ligands, including two bridging carboxylates in a carboxylate O,O' mode, one chelating carboxylate in a η²-mode, and one monodentate carboxylate for each Zn atom (Figure 1a). The Zn₂ SBUs are linked via an imidazolium tricarboxylate to form a 2D framework (Figure 1b). If the Zn₂ dimeric unit and the DCPCBim ligand are simplified as 6- and 3-connected nodes, respectively, the framework can be simplified as a 2D binodal 3,6-connected net with the point (Schläfli) symbol (4².6)₂(4⁴.6⁹.8²) with the 6- and 3-connected nodes in a ratio of 1:2 (Figure 1e). This represents an unprecedented 2D network topology with intralayer porosity⁹ rather than interlayer porosity.¹⁰ The overall charge of the framework is in balance, and the framework is of a charge-separated nature (see below). The 1D intralayer channels exist along the *b* axis, as shown in Figures 1b,c, and the solvated DMF molecules reside in the channels (Figures 1f,g). The 2D flat layers slide in two directions to stack in an ABCA'B'C' packing mode and are repeated every six layers (Figure 1d). The adjacent 2D layers are packed via offset face-to-face π–π interactions between para-substituted phenyl rings with an interplanar distance of 3.43 Å. The distance between the adjacent 2D layers is 6.44 Å. Upon removal of the solvated molecules, there is 17.3% void space to the total crystal volume (total potential solvent area volume 657.5 Å³ per unit cell volume 3808.4 Å³) calculated using PLATON.¹¹

Framework Charges. A density functional theory (DFT) study was undertaken to calculate the atomic charges in the framework (Figure 2). The charge of each atom is given in Table 1. The results of group charges are shown in Table 2, which were calculated by assigning the atoms to different groups and summing the charges of the appropriate atoms. For the imidazolium ring, the C atoms of the imidazolium ring are mostly negatively charged; corresponding H atoms are positively charged; the N atoms of the imidazolium ring possess negative charge. The total charge of the imidazolium ring is 0.452e. The imidazolium ring carries less positive charge than its usual form because the imidazolium ring receives charges from the benzene ring –Ph(–iso) and –COO(–iso). Most of the negative charge is distributed on the –COO(–iso) segments (–1.449 and –0.59e), indicating the strongest electron-donating potential of the carboxylate segment. When the central Zn²⁺ ion is coordinated by the carboxylate of the ligand, Zn²⁺ receives charges from each ligand, and charge

transfer may occur among the Zn²⁺ cation, carboxylate, and conjugated imidazolium and benzene rings. As a result, the phenyl rings carry positive charges.

The acidity of H atoms in the imidazolium ring, particularly that at C2, is important for quantifying the effect of the imidazolium ring. The H atom at C2 is more acidic than those at C4/C5. Because the H(C2) atom is positively charged, attractive interaction to guest anions or gas molecules may be expected.¹²

Phase Purity and Thermostability. Powder X-ray diffraction (PXRD) was used to confirm the phase purity of DCPCBim-MOF-Zn, as shown in Figure 3. The patterns of the as-synthesized product closely match the simulated ones of single-crystal analysis, which are indicative of the pure solid-state phase.

Thermogravimetric analysis (TGA) of DCPCBim-MOF-Zn shows a weight loss of 7.99% from room temperature to 250 °C corresponding to the loss of one guest DMF (calcd 7.78%; Figure 4a). There is no weight loss from 250 to 400 °C. The framework may decompose above 400 °C.

Porosity and Physisorption Studies. As shown above, the presence of DMF in the pore channels has been unambiguously confirmed by X-ray structural determination, IR, TGA, and microanalysis. The included guests were further analyzed by X-ray photoelectron microscopy (XPS) and energy-dispersive spectrometry (EDS). XPS reveals that nitrate anions are absent but a trace amount of Cl[–] anions are present in the pore channels (Figures S1–S3 in the Supporting Information, SI). The presence of Cl[–] anions is probably attributed to the charge-separated nature, and a CH⋯Cl hydrogen bond is likely to be established between the imidazolium ring and Cl[–].¹² XPS and EDS analyses showed that the atomic percentage of chloride (Cl 2p) for DCPCBim-MOF-Zn decreased (from 2.01% to 0.22% as revealed by XPS) after the as-synthesized product was treated by solvent exchange in MeOH for 24 h, which indicates that most of the Cl[–] ions in the as-synthesized product were removed.

To testify the porosity of DCPCBim-MOF-Zn, sorption isotherms have been measured on a thermally activated sample for gases and vapors.¹³ Prior to gas adsorption measurements, DCPCBim-MOF-Zn was activated by heating in a vacuum for 24 h at 150 °C after solvent exchange in MeOH for 24 h. TGA (Figure 4b) and IR [disappearance of the ν(C=O) vibration at around 1673 cm^{–1}] showed that guest DMF molecules residing in the channels were completely removed. The PXRD patterns of guest-free DCPCBim-MOF-Zn indicated that the bulk sample well retained the crystallinity, confirmed by the stability of the framework in the absence of guest molecules (Figure 3c).

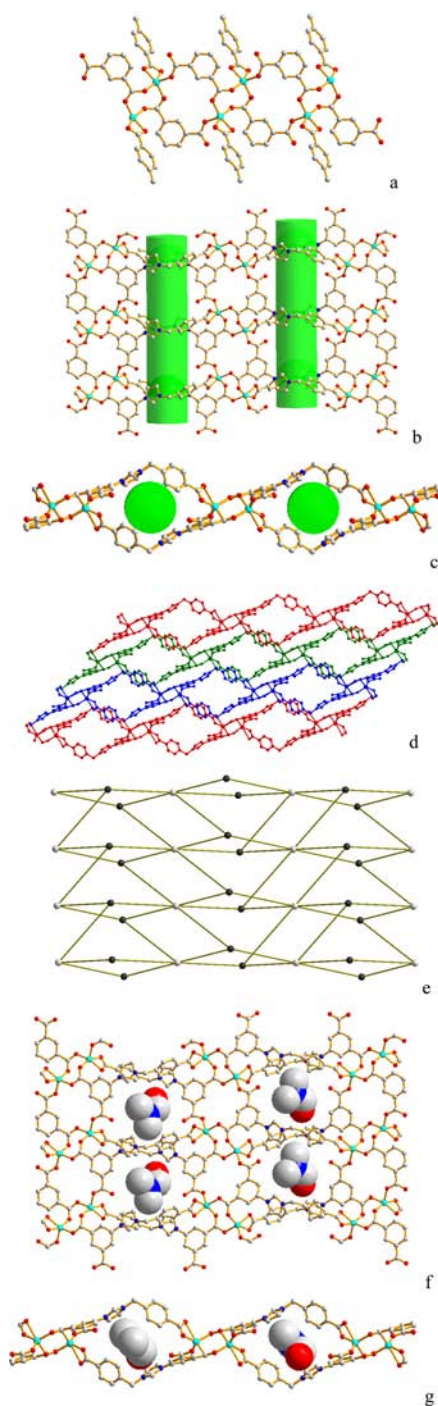


Figure 1. X-ray structures of DCPCBim-MOF-Zn showing (a) a view of the structure with Zn₂ dimeric units, (b and c) views of the 1D channels along the *b* axis, (d) packing of the 2D layers in the (101) plane, (e) a (4².6)₂(4⁴.6⁹.8²) topological diagram, and (f and g) DMF molecules residing in the 1D channels.

Therefore, the excellent framework stability provides an opportunity to study its permanent porosity featured in the charge-separated character.

A N₂ adsorption isotherm was first measured as showing neglectable uptake by the framework even at low temperature (Figure 5). Such a behavior has been reported for some MOFs.¹⁴ However, CO₂ adsorption of DCPCBim-MOF-Zn at 195 K revealed a type I profile with a steep uptake at low relative-pressure regions. The adsorption capacity at 1 atm is

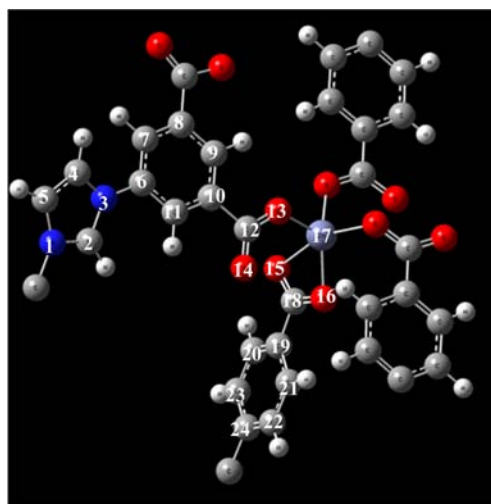


Figure 2. Model cluster of DCPCBim-MOF-Zn for DFT calculation (Zn, pale blue; O, red; N, blue; C, gray; H, white).

56.2 cm³ g⁻¹ (11.0 wt %) at 195 K, corresponding to 1.1 CO₂ molecules per DCPCBim ligand. The Langmuir and Brunauer–Emmett–Teller (BET) surface areas calculated from the CO₂ profile are 245 and 222 m² g⁻¹, respectively. According to the Horvath–Kawazoe method, the pore volume was calculated as 0.104 cm³ g⁻¹ and the pore width is centered around 3.7 Å. Interestingly, the isotherms show remarkable hysteresis loops between the adsorption and desorption branches even at 298 K. This is unusual because hysteresis loops are usually temperature-dependent and tend to be unobscured with increasing temperature.¹⁵ For example, an indium carboxylate framework NOTT-202 exhibits adsorption–desorption hysteresis only when the temperature is below the triple point of CO₂.^{15b} The hysteresis confines the gas molecules within the pores at high pressure and releases them at low pressure, thus potentially enhancing gas uptake for potential application. The strong interaction of CO₂ with the framework is reflected in the high value of *Q*_{st} (ca. 30 kJ mol⁻¹) calculated from the isotherms at 273 and 298 K using the Clausius–Clapeyron equation. The value is comparable to those of Cu₃(BTC)₂ (BTC = 1,3,5-benzenetricarboxylate, HKUST-1) and others with exposed metal sites.¹⁶ Therefore, the hysteretic sorption and large *Q*_{st} suggest a strong interaction of CO₂ molecules with the narrowed and charge-separated framework.¹⁷ This is different from previous observations that the hysteretic gas adsorption behavior is induced by partial double interpenetration^{15b} or guest cations within the pore channels (i.e., the gas is kinetically trapped in the framework).¹⁸

The activated DCPCBim-MOF-Zn after MeOH exchange was also tested for H₂ and CH₄ uptake (Figure 6), which revealed H₂ uptake up to 66.4 cm³ g⁻¹ (at 77 K and 1 atm) and CH₄ uptake of 52.8 cm³ g⁻¹ (at 195 K and 1 atm), corresponding to 1.3 H₂ and 1.0 CH₄ molecules per ligand, respectively. Interestingly, prominent hysteresis was also observed in both the adsorption profiles, suggesting strong interactions of H₂/CH₄ molecules with the charge-separated framework. H₂ coverage dependencies of the isosteric heat of adsorption (*Q*_{st}) were calculated from fits of 77 and 87 K isotherms. The estimated *Q*_{st} is approximately 9.3 kJ mol⁻¹ at low surface coverage with the virial-fit approach. The *Q*_{st} value drops off from 9.3 to 5.5 kJ mol⁻¹ with H₂ uptake, representing

Table 1. Atomic Charges on the Fragment Cluster in Figure 2^a

atom no.	1	2	3	4	5	6	7
charges	-0.088 (N)	-0.073 (C)	-0.084 (N)	0.070 (C)	-0.155 (C)	0.403 (C)	-0.206 (C)
atom no.	8	9	10	11	12	13	14
charges	0.412 (C)	-0.284 (C)	-0.014 (C)	-0.239 (C)	-0.014 (C)	-0.16 (O)	-0.416 (O)
atom no.	15	16	17	18	19	20	21
charges	-0.129 (O)	-0.154 (O)	0.163 (Zn)	0.463 (C)	0.797 (C)	-0.093 (C)	0.393 (C)
atom no.	22	23	24	H(C2)	H(C4)	H(C5)	H(C7)
charges	-0.596 (C)	-0.449 (C)	0.808 (C)	0.239	0.264	0.264	0.196
atom no.	H(C9)	H(C11)	H(C20)	H(C21)	H(C22)	H(C23)	
charges	0.284	0.225	0.172	0.168	0.139	0.141	

^aCharges in e (atomic units).

Table 2. Partial Charges on the Different Segments of DCPCBim-MOF-Zn

group	charge	group	charge
imi ring	0.452	-COO(p)	0.18
-Ph(iso)	1.016	-COO (iso)-1	-0.59
-Ph(p)	1.48	-COO (iso)-2	-1.449
central Zn	0.135		

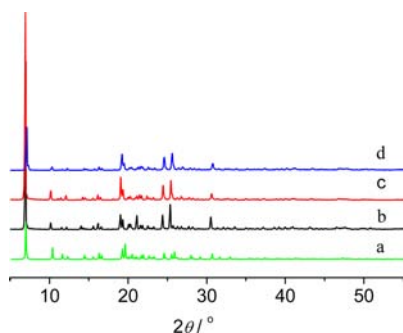


Figure 3. Comparison of PXRD patterns of DCPCBim-MOF-Zn: (a) simulated pattern based on the single-crystal structure; (b) as-synthesized product; (c) guest-free form after solvent exchange in MeOH for 24 h and subsequent vacuum drying for 24 h at 150 °C; (d) guest-free form after sorption.

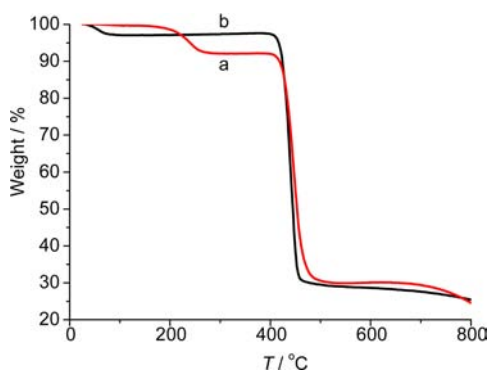


Figure 4. TGA curves of DCPCBim-MOF-Zn recorded under a N₂ atmosphere: (a) as-synthesized; (b) guest-free form after solvent exchange in MeOH for 24 h and subsequent vacuum drying for 24 h at 150 °C.

one of the highest values at low surface coverage for hydrogen physisorption in porous materials.¹⁹

The above results suggest that DCPCBim-MOF-Zn after MeOH exchange may be able to exhibit adsorption selectivity for CO₂/H₂/CH₄ over N₂. Exclusion of N₂ molecules over

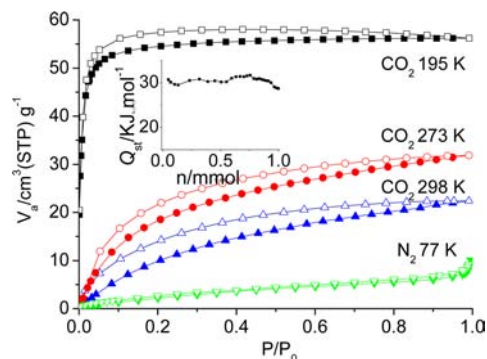


Figure 5. N₂ adsorption–desorption isotherm measured at 77 K and CO₂ isotherms measured at 195, 273, and 298 K for activated DCPCBim-MOF-Zn after MeOH exchange. Filled and open symbols represent adsorption and desorption, respectively. Inset: isosteric heat of adsorption for CO₂.

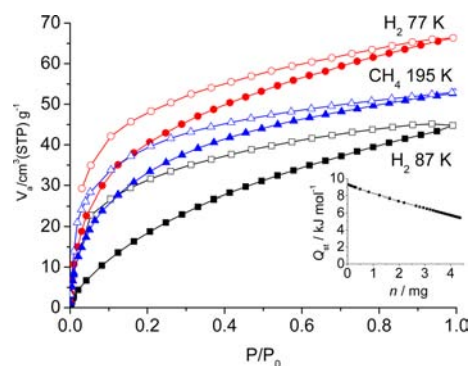


Figure 6. CH₄ adsorption–desorption isotherm measured at 195 K and H₂ adsorption–desorption isotherms measured at 77 and 87 K for activated DCPCBim-MOF-Zn after MeOH exchange. Filled and open symbols represent adsorption and desorption, respectively. Inset: isosteric heat of adsorption for H₂.

various gases is useful in a number of industrial processes; for example, selective adsorption of H₂ over N₂ is an important concern because of its potential application for H₂ enrichment from N₂/H₂ exhaust mixtures in ammonia synthesis.²⁰ Among several factors that may be responsible for the selective adsorptions, including molecular sieving, coordinatively unsaturated metal centers, appropriate pore size, and host–guest interactions,²¹ the present selectivity may be contributed by preferential host–guest interactions caused by the charge-separation framework. Except the H₂ gas with the smallest kinetic diameter, adsorbate gases like CO₂ or CH₄ with higher polarizabilities can well interact with the present framework,

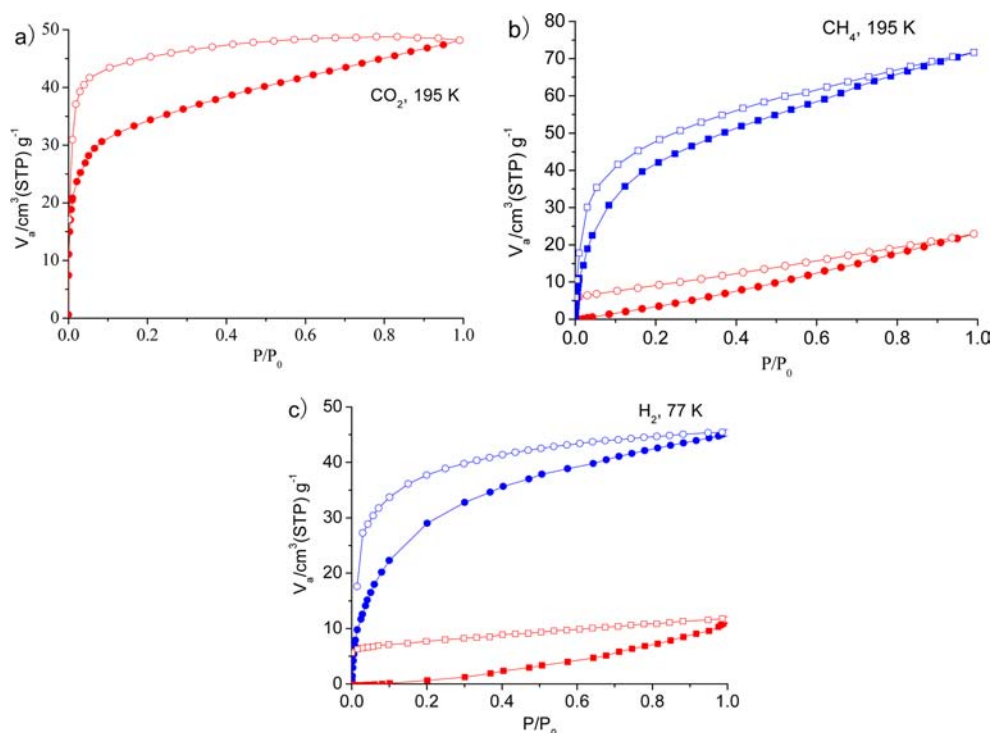


Figure 7. (a) CO_2 adsorption–desorption isotherm measured at 195 K, (b) CH_4 adsorption–desorption isotherms measured at 195 K, and (c) H_2 adsorption–desorption isotherms measured at 77 K for activated **DCPCBim-MOF-Zn** (as-prepared crystalline sample, red). The isotherms of activated **DCPCBim-MOF-Zn** after MeOH exchange are shown as a comparison (blue; a different batch of sample from that in Figure 5 was used for measurement). Filled and open symbols represent adsorption and desorption, respectively.

but N_2 with lower polarizability may be excluded from the pore channel.²²

Further studies show that trace Cl^- anions significantly change the gas-sorption behavior (Figure 7). As discussed above, trace Cl^- anions were present in the as-prepared crystalline sample of **DCPCBim-MOF-Zn**, which was washed with MeOH three times to clean the surface and subsequently activated by heating in a vacuum for 24 h at 150 °C. CO_2 adsorption at 195 K revealed a significantly lower amount of ca. $30 \text{ cm}^3 \text{ g}^{-1}$ at low relative pressure regions ($P/P_0 < 0.1$). The adsorption amount gradually increases to $48.2 \text{ cm}^3 \text{ g}^{-1}$ at 1 atm, which is slightly lower than that of activated **DCPCBim-MOF-Zn** with lower chloride content. This shows that CO_2 molecules are more difficult to enter the pore channels. The presence of trace Cl^- anions also decreases remarkably the absorbed amount of CH_4 or H_2 molecules, and only neglectable uptake of either gas molecules was observed. These results suggest that guest anions can modulate the sorption property of the present material.¹⁸ This behavior is closely related to the charge-separated nature of **DCPCBim-MOF-Zn**. A trace amount of Cl^- ions may be readily entrapped in the pore channels and block H_2 or CH_4 molecules from passing into the pore channel. In comparison, the affinity toward CO_2 is probably due to the quadrupolar nature of CO_2 . The electric field in the host framework interacts with the quadrupole moment of CO_2 to make an additional contribution to the potential energy of adsorption.²³

Because charge separation may produce a strong effect for polar guests, the uptake of methanol and ethanol vapors was performed for **DCPCBim-MOF-Zn** after MeOH exchange (Figure 8). MeOH sorption isotherm showed a type I profile with a steep uptake in the low-pressure region at 298 K. The adsorption capacity is $60.2 \text{ cm}^3 \text{ g}^{-1}$ corresponding to 1.2

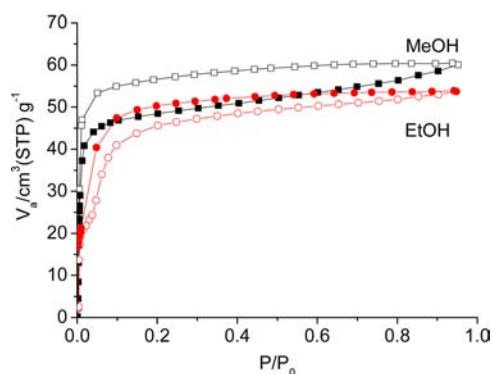


Figure 8. MeOH and EtOH adsorption–desorption isotherms of **DCPCBim-MOF-Zn** measured at 298 K. Filled and open symbols represent adsorption and desorption, respectively.

MeOH molecules per formula unit of ligand. Differently, the EtOH adsorption isotherm revealed double steps in the adsorption branch. The initial uptake is due to the micropore filling in the micropores and is followed by a second filling. The first step of $20.0 \text{ cm}^3 \text{ g}^{-1}$ corresponds to 0.45 EtOH molecules per formula unit of ligand, while the total of $50.7 \text{ cm}^3 \text{ g}^{-1}$ corresponds to 0.97 EtOH molecules. The stepwise sorption may indicate a structural transformation of the 2D framework induced by ethanol inclusion.^{5a} Similar to the gas-sorption behavior, both the MeOH and EtOH isotherms show large hysteresis, further verifying that the strong interaction arises from charge separation of the framework.

Luminescence Properties. The solid-state emission spectra of **DCPCBim-MOF-Zn** and the free ligand at room temperature are shown in Figure 9. **DCPCBim-MOF-Zn** and the free ligand display blue fluorescence with maximum

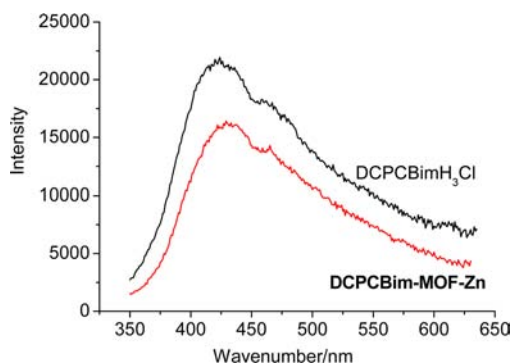


Figure 9. Solid-state photoluminescence spectra of DCPCBim-MOF-Zn ($\lambda_{\text{ex}} = 317$ nm) and DCPCBimH₃Cl ($\lambda_{\text{ex}} = 323$ nm).

emission at 429 and 424 nm upon excitation at 317 and 323 nm, respectively. Because the emission band of DCPCBim-MOF-Zn occurs at a position similar to that of the free ligand with a rather resembling band profile, the emission of DCPCBim-MOF-Zn should be originated from an intraligand $\pi \rightarrow \pi^*$ transition of the ligand.

CONCLUSION

In summary, a 2D MOF has been synthesized from Zn²⁺ ions and imidazolium tricarboxylate ligands characteristic of charge separation. The 2D MOF exhibits an unprecedented 3,6-connected net topology with the point (Schläfli) symbol (4².6)₂(4⁴.6⁹.8²). The framework has 1D intralayer channels with a highly polar pore surface. DFT calculations show that the positive charge is located on the imidazolium/phenyl rings and the negative charge is on the coordinated carboxylate moieties. The evacuated framework adsorbs gas molecules with high polarizabilities (CO₂, H₂, and CH₄) and polar solvent vapors. About one guest molecule is absorbed for each zinc-ligand moiety. The pronounced hysteresis and high adsorption enthalpy indicate that strong interaction exists between the framework and guest molecules, which arises from the charge-separated nature of the MOF channels. Additionally, the presence of trace Cl⁻ anions in the pore channels significantly changes the sorption properties; H₂ and CH₄ are excluded and only CO₂ is allowed to enter the pore channels at higher relative pressure. The present strategy may be useful to find new adsorbents with hysteretic adsorption at high temperatures for practical applications.

EXPERIMENTAL SECTION

Materials and Methods. All starting materials and solvents were obtained from commercial sources and used without further purification. PXRD data were recorded on a Bruker D8 Advance diffractometer at 40 kV and 40 mA with a Cu-target tube and a graphite monochromator. IR spectra were measured on a Nicolet/Nexus-670 FT-IR spectrometer with KBr pellets. TGA was performed under N₂ at a heating rate of 10 °C min⁻¹ on a Netzsch Termo Microbalance TG 209 F3 Tarsus. XPS spectra were recorded on a Thermo Fisher Scientific ESCALAB 250 spectrometer with X-ray-monochromatized Al K α radiation. The sorption isotherms were measured with a Quantachrome Autosorb-iQ or Autosorb-iQ2 analyzer.

Dimethyl 5-(1*H*-imidazol-1-yl)isophthalate. Glyoxal (1.6 mL, 30%) was added dropwise into dimethyl 5-aminoisophthalate (10 mmol, 2.09 g) in MeOH (30 mL), and the reaction mixture was stirred for 24 h. NH₄Cl (3.21 g, 60 mmol) was added to the resultant pale-yellow suspension. After 1 h, a 37% aqueous HCHO solution (3.2 mL) was added and refluxed for 1 h. H₃PO₄ (4.2 mL) was added dropwise. The mixture was refluxed for 48 h. The solvent was removed under

reduced pressure, and icy water was added to dissolve the residue. The pH was adjusted to 9 with a 40% KOH solution and extracted with CH₂Cl₂. The organic layer was washed with water and a saturated NaCl solution in turn, dried over anhydrous MgSO₄, and evaporated to dryness to obtain a yellow solid (yield 80%). ¹H NMR (300 MHz, DMSO): δ 8.43 (s, 1H), 8.38 (d, $J = 1.3$ Hz, 1H), 8.36 (s, 2H), 7.93 (s, 1H), 7.13 (s, 1H), 3.92 (s, 6H).

***N*-(Dimethyl-3,5-benzenedicarboxylate)-*N'*-(methyl-4-benzylcarboxylate)imidazolium Bromide.** A solution of dimethyl 5-(1*H*-imidazol-1-yl)isophthalate (1.04 g, 4 mmol) and methyl 4-(bromomethyl)benzoate (1.37 g, 6 mmol) in MeCN (40 mL) was stirred at room temperature for 3 days. The solvent was removed under vacuum and recrystallized from EtOH/Et₂O to obtain a gray solid (1.06 g, yield 66%). ¹H NMR (300 MHz, DMSO-*d*₆): δ 10.09 (s, 1H), 8.57 (s, 3H), 8.50 (s, 1H), 8.02 (d, $J = 4.5$ Hz, 2H), 7.98 (s, 1H), 7.62 (d, $J = 8.2$ Hz, 2H), 5.60 (s, 2H), 3.95 (s, 6H), 3.85 (s, 3H).

***N*-(3,5-Dicarboxylphenyl)-*N'*-(4-carboxylbenzyl)imidazolium Chloride (DCPCBimH₃Cl).** *N*-(Dimethyl-3,5-benzenedicarboxylate)-*N'*-(methyl-4-benzylcarboxylate)imidazolium bromide (409 mg, 0.8 mmol) was dissolved in a 20% HCl aqueous solution (20 mL) and refluxed for 12 h, resulting in precipitation of imidazolium chloride. The mixture was filtered to give a white powder (252 mg, yield 75%). ¹H NMR (300 MHz, DMSO-*d*₆): δ 10.12 (s, 1H), 8.55 (s, 1H), 8.51 (s, 3H), 8.02 (s, 1H), 7.97 (d, $^3J_{\text{H-H}} = 8.13$ Hz, 2H), 7.61 (d, $^3J_{\text{H-H}} = 8.2$ Hz, 2H), 5.58 (s, 2H). IR (KBr pellets, cm⁻¹): 3060br, 2910br, 1714s, 1614w, 1572w, 1552m, 1447w, 1420m, 1405m, 1375m, 1309w, 1244m, 1214s, 1184m, 1138w, 1107w, 1084m, 1022w, 852w, 795w, 750m, 721m, 689m, 669w, 656w, 616w.

Synthesis of {[Zn₂(DCPCBim)₂]·DMF}_n (DCPCBim-MOF-Zn). DCPCBimH₃Cl (10 mg, 0.025 mmol) in DMF (3 mL) and Zn(NO₃)₂·6H₂O (15 mg, 0.05 mmol) in H₂O (1 mL) were mixed, and the mixture was heated in a closed container at 80 °C. After 2 days, colorless crystals were obtained (9.3 mg, yield 40% based on L). Microanal. Found (calcd) for C₄₁H₃₃Zn₂N₅O₁₃·H₂O: C, 51.37 (51.81); H, 3.42 (3.50); N, 7.23 (7.37). IR (KBr pellets, cm⁻¹): 3433br, 3085m, 1673m (DMF), 1644m, 1623s, 1582s, 1512w, 1448m, 1421s, 1373s, 1347s, 1228w, 1159w, 1082m, 861w, 783m, 745m, 720m, 617w, 574w, 458w.

X-ray Structure Determination. X-ray crystallographic intensity data were collected for DCPCBim-MOF-Zn using an Oxford Gemini S Ultra diffractometer equipped with a graphite-monochromated Enhance (Cu) X-ray source ($\lambda = 1.54178$ Å). The structure was solved by direct methods following difference Fourier syntheses and refined by a full-matrix least-squares method against F_o^2 using SHELXTL software.²⁴ All non-H atoms were refined with anisotropic thermal parameters, while the H atoms on the ligands were placed in idealized positions with isotropic thermal parameters. Appropriate restraints were applied to model the disordered DMF molecule to the idealized geometry.

Crystallographic data for DCPCBim-MOF-Zn: C₄₁H₃₁Zn₂N₅O₁₃, fw = 932.45, monoclinic, C2/c, $a = 25.843(3)$ Å, $b = 8.6601(4)$ Å, $c = 17.4254(11)$ Å, $\alpha = 90^\circ$, $\beta = 102.435(9)^\circ$, $\gamma = 90^\circ$, $V = 3808.4(5)$ Å³, $Z = 4$, $T = 150(2)$ K, $\lambda = 1.54178$ Å, $\rho_{\text{calcd}} = 1.626$ mg m⁻³, $\mu = 2.216$ mm⁻¹, 5175 reflections were collected (2726 were unique) for $5.20 < \theta < 59.99$, $R(\text{int}) = 0.0548$, $R1 = 0.0824$, $wR2 = 0.2188$ [$I > 2\sigma(I)$], $R1 = 0.0911$, $wR2 = 0.2298$ (all data) for 290 parameters, and GOF = 1.031. CCDC 892909.

Calculation of Framework Charges in DCPCBim-MOF-Zn.

The atomic charges of the framework atoms were calculated from DFT on the basis of the fragment cluster, as illustrated in Figure 2. On the basis of the ChelpG method, DFT calculations using the Lee–Yang–Parr correlation functional (B3LYP) were carried out with the Gaussian 09 package. To compute the atomic partial charges, two kinds of basis sets were employed: For Zn, the LANL2DZ basis set was used, and 6-31+G* was employed for the rest of the atoms. For the cleaved clusters of Zn, the terminations are connected with Zn atoms in the real system, and they were saturated by light metal Li atoms. Saturated alkanes were terminated with -CH₃.²⁵

■ ASSOCIATED CONTENT

■ Supporting Information

X-ray crystallographic data in CIF format, XPS spectra, EDS patterns, and CO₂ sorption isotherms. This material is available free of charge via the Internet at <http://pubs.acs.org>.

■ AUTHOR INFORMATION

Corresponding Author

*E-mail: zhijyong@mail.sysu.edu.cn (J.Z.), cesscy@mail.sysu.edu.cn (C.-Y.S.).

Notes

The authors declare no competing financial interest.

■ ACKNOWLEDGMENTS

We gratefully acknowledge the 973 Program (Grant 2012CB821701), the NSFC Projects of China (Projects 20903121, 21273007, 21173272, U0934003, and 91222201), the NSF of Guangdong Province (Grant S2011010001307), and the RFDP of Higher Education of China and the Fundamental Research Funds for the Central Universities.

■ REFERENCES

- (1) (a) Kitagawa, S.; Kitaura, R.; Noro, S.-i. *Angew. Chem., Int. Ed.* **2004**, *43*, 2334. (b) Férey, G. *Chem. Soc. Rev.* **2008**, *37*, 191. (c) Lee, J. Y.; Farha, O. K.; Roberts, J.; Scheidt, K. A.; Nguyen, S. T.; Hupp, J. T. *Chem. Soc. Rev.* **2009**, *38*, 1450. (d) Murray, L. J.; Dincă, M.; Long, J. R. *Chem. Soc. Rev.* **2009**, *38*, 1294. (e) Kuppler, R. J.; Timmons, D. J.; Fang, Q.-R.; Li, J.-R. M.; T., A.; Young, M. D.; Yuan, D.; Zhao, D.; Zhuang, W.; Zhou, H.-C. *Coord. Chem. Rev.* **2009**, *253*, 3042. (f) Farrusseng, D.; Aguado, S.; Pinel, C. *Angew. Chem., Int. Ed.* **2009**, *48*, 7502. (g) Corma, A.; García, H.; Llabrés, I.; Xamena, F. X. *Chem. Rev.* **2010**, *110*, 4606. (h) Morris, R. E.; Wheatley, P. S. *Angew. Chem., Int. Ed.* **2008**, *47*, 4966. (i) Li, J.-R.; Kuppler, R. J.; Zhou, H.-C. *Chem. Soc. Rev.* **2009**, *38*, 1477. (j) Yaghi, O. M.; O'Keeffe, M.; Ockwig, N. W.; Chae, H. K.; Eddaoudi, M.; Kim, J. *Nature* **2003**, *423*, 705.
- (2) Liu, J.; Thallapally, P. K.; McGrail, B. P.; Brown, D. R.; Liu, J. *Chem Soc. Rev.* **2012**, *41*, 2308.
- (3) (a) Babarao, R.; Jiang, J. W.; Sandler, S. I. *Langmuir* **2009**, *25*, 5239. (b) Botas, J. A.; Calleja, G.; Sanchez-Sanchez, M.; Orcajo, M. G. *Langmuir* **2010**, *26*, 5300. (c) Xiang, Z. H.; Hu, Z.; Cao, D. P.; Yang, W. T.; Lu, J. M.; Han, B. Y.; Wang, W. C. *Angew. Chem., Int. Ed.* **2011**, *50*, 491.
- (4) Bae, Y. S.; Farha, O. K.; Hupp, J. T.; Snurr, R. Q. *J. Mater. Chem.* **2009**, *19*, 2131.
- (5) (a) Higuchi, M.; Tanaka, D.; Horike, S.; Sakamoto, H.; Nakamura, K.; Takashima, Y.; Hijikata, Y.; Yanai, N.; Kim, J.; Kato, K.; Kubota, Y.; Takata, M.; Kitagawa, S. *J. Am. Chem. Soc.* **2009**, *131*, 10336. (b) Zheng, S.-T.; Bu, J. T.; Li, Y.; Wu, T.; Zuo, F.; Feng, P.; Bu, X. *J. Am. Chem. Soc.* **2010**, *132*, 17062.
- (6) (a) Crees, R. S.; Cole, M. L.; Hanton, L. R.; Sumbly, C. J. *Inorg. Chem.* **2010**, *49*, 1712. (b) Lee, J. Y.; Roberts, J. M.; Farha, O. K.; Sarjeant, A. A.; Scheidt, K. A.; Hupp, J. T. *Inorg. Chem.* **2009**, *48*, 9971. (c) Roberts, J. M.; Farha, O. K.; Sarjeant, A. A.; Hupp, J. T.; Scheidt, K. A. *Cryst. Growth Des.* **2011**, *11*, 4747.
- (7) (a) Oisaki, K.; Li, Q.; Furukawa, H.; Czaja, A. U.; Yaghi, O. M. *J. Am. Chem. Soc.* **2010**, *132*, 9262. (b) Kong, G. Q.; Xu, X.; Zou, C.; Wu, C. D. *Chem. Commun.* **2011**, *47*, 11005. (c) Chun, J.; Lee, H. S.; Jung, I. G.; Lee, S. W.; Kim, H. J.; Son, S. U. *Organometallics* **2010**, *29*, 1518. (d) Chun, J.; Jung, G.; Kim, H. J.; Park, M.; Lah, M. S.; Son, S. U. *Inorg. Chem.* **2009**, *48*, 6353.
- (8) (a) Han, L.; Zhang, S.; Wang, Y.; Yan, X.; Lu, X. *Inorg. Chem.* **2009**, *48*, 786. (b) Fei, Z.; Geldbach, T. J.; Scopelliti, R.; Dyson, P. J. *Inorg. Chem.* **2006**, *45*, 6331.
- (9) (a) Wang, Q.; Zhang, J.; Zhuang, C.-F.; Tang, Y.; Su, C.-Y. *Inorg. Chem.* **2009**, *48*, 287. (b) Zheng, S.-R.; Yang, Q.-Y.; Liu, Y.-R.; Zhang, J.; Tong, Y.-X.; Zhao, C.-Y.; Su, C.-Y. *Chem. Commun.* **2008**, 356.
- (10) (a) Fukushima, T.; Horike, S.; Inubushi, Y.; Nakagawa, K.; Kubota, Y.; Takata, M.; Kitagawa, S. *Angew. Chem., Int. Ed.* **2010**, *49*, 4820. (b) Kondo, A.; Noguchi, H.; Ohnishi, S.; Kajiro, H.; Tohdoh, A.; Hattori, Y.; Xu, W.-C.; Tanaka, H.; Kanoh, H.; Kaneko, K. *Nano Lett.* **2006**, *6*, 2581. (c) Kondo, A.; Kajiro, H.; Noguchi, H.; Carlucci, L.; Proserpio, D. M.; Ciani, G.; Kato, K.; Takata, M.; Seki, H.; Sakamoto, M.; Hattori, Y.; Okino, F.; Maeda, K.; Ohba, T.; Kaneko, K.; Kanoh, H. *J. Am. Chem. Soc.* **2011**, *133*, 10512. (d) Wang, X.; Feng, J.; Huang, J.; Zhang, J.; Pan, M.; Su, C.-Y. *CrystEngComm* **2010**, *12*, 725.
- (11) Spek, L. *PLATON: A Multipurpose Crystallographic Tool*; Utrecht University: Utrecht, The Netherlands, 2001.
- (12) (a) Crowhurst, L.; Mawdsley, P. R.; Perez-Arlandis, J. M.; Salter, P. A.; Welton, T. *Phys. Chem. Chem. Phys.* **2003**, *5*, 2790. (b) Grondin, J.; Lassègues, J.-C.; Cavagnat, D.; Buffeteau, T.; Johansson, P.; Holomb, R. J. *Raman Spectrosc.* **2011**, *42*, 733. (c) Köddermann, T.; Wertz, C.; Heintz, A.; Ludwig, R. *ChemPhysChem* **2006**, *7*, 1944. (d) Yokozeki, A.; Kasprzak, D. J.; Shiflett, M. B. *Phys. Chem. Chem. Phys.* **2007**, *36*, 5018.
- (13) The isotherms have good repeatability measured on the same batch or different batches of samples for several times (see Figures 5, 6, and S4 and S5 in the SI).
- (14) (a) Pan, L.; Adams, K. M.; Hernandez, H. E.; Wang, X.; Zheng, C.; Hattori, Y.; Kaneko, K. *J. Am. Chem. Soc.* **2003**, *125*, 3062. (b) Otsubo, K.; Wakabayashi, Y.; Ohara, J.; Yamamoto, S.; Matsuzaki, H.; Okamoto, H.; Nitta, K.; Uruga, T.; Kitagawa, H. *Nat. Mater.* **2011**, *10*, 291.
- (15) (a) Kanoo, P.; Reddy, S. K.; Kumari, G.; Haldar, R.; Narayana, C.; Balasubramanian, S.; Maji, T. K. *Chem. Commun.* **2012**, *48*, 8487. (b) Yang, S.; Lin, X.; Lewis, W.; Suetin, M.; Bichoutskaia, E.; Parker, J. E.; Tang, C. C.; Allan, D. R.; Rizkallah, P. J.; Hubberstey, P.; Champness, N. R.; Thomas, K. M.; Blake, A. J.; Schröder, M. *Nat. Mater.* **2012**, *11*, 710.
- (16) (a) Liang, Z.; Marshall, M.; Chaffee, A. L. *Energy Fuels* **2009**, *23*, 2785. (b) Kanoo, P.; Haldar, R.; Cyriaca, S. T.; Maji, T. K. *Chem. Commun.* **2011**, *47*, 11038.
- (17) Keskin, S.; van Heest, T. M.; Sholl, D. S. *ChemSusChem* **2010**, *3*, 879.
- (18) (a) Yang, S.; Lin, X.; Blake, A. J.; Walker, G. S.; Hubberstey, P.; Champness, N. R.; Schröder, M. *Nat. Chem.* **2009**, *1*, 487. (b) Lin, Z.-J.; Liu, T.-F.; Huang, Y.-B.; Lü, J.; Cao, R. *Chem.—Eur. J.* **2012**, *18*, 7896.
- (19) Murray, L. J.; Dincă, M.; Long, J. R. *Chem. Soc. Rev.* **2009**, *38*, 1294.
- (20) Yang, R. T. *Adsorbents: Fundamentals and Applications*; John Wiley & Sons: Hoboken, NJ, 2003.
- (21) (a) Hazra, A.; Kanoo, P.; Maji, T. K. *Chem. Commun.* **2011**, *47*, 538. (b) Dincă, M.; Long, J. R. *J. Am. Chem. Soc.* **2005**, *127*, 9376. (c) Kanoo, P.; Ghosh, A. C.; Cyriac, S. T.; Maji, T. K. *Chem.—Eur. J.* **2012**, *18*, 237.
- (22) Rallapalli, P.; Prasanth, K.; Patil, D.; Somani, R.; Jasra, R.; Bajaj, H. J. *Porous Mater.* **2011**, *18*, 205.
- (23) Maji, T. K.; Matsuda, R.; Kitagawa, S. *Nat. Mater.* **2007**, *6*, 142.
- (24) Sheldrick, G. M. *SHELX-97: Program for Crystal Structure Solution and Refinement*; University of Göttingen: Göttingen, Germany, 1997.
- (25) Zheng, C.; Liu, D.; Yang, Q.; Zhong, C.; Mi, J. *Ind. Eng. Chem. Res.* **2009**, *48*, 10479.